Impact of surface roughness of Au core in Au/Pd core—shell nanoparticles toward formic acid oxidation — Experiment and simulation

Chiajen Hsu, Chienwen Huang, Yaowu Hao, Fuqiang Liu*

Department of Materials Science and Engineering, University of Texas at Arlington, Arlington, TX 76019, USA

HIGHLIGHTS

- Unique Au/Pd core—shell nanoparticles were synthesized via a galvanic replacement of Cu by Pd on hollow Au.
- Au/Pd core—shell nanoparticles with smooth Au surface by adding Na_2SO_3 demonstrated highly catalytic activity and durability.
- Simulation studies demonstrated that the Au/Pd core—shell nanoparticles achieved higher formate and lower hydroxyl coverage.

ARTICLE INFO

ABSTRACT

The Au/Pd core—shell nanoparticles (NPs) were synthesized via galvanic replacement of Cu by Pd on hollow Au cores by adding different concentrations of Na_2SO_3 solution. It was found that the higher concentration of Na_2SO_3 that was used, the rougher the Au nanospheres became. However, the rougher Au surface may cause more defects in the Pd layers and decrease the catalytic abilities. The Au/Pd NPs synthesized using 0 M Na_2SO_3 (denoted as 0 M-Au/Pd NPs) have the smoothest Pd surface and demonstrate higher formic acid oxidation (FAO) activity (0.714 mA cm^{-2}, normalized to the surface area of Pd) than other Au/Pd NPs and commercial Pd black (0.47 mA cm^{-2}). Additional electrochemical characterization of the 0 M-Au/Pd NPs also demonstrated lower CO-stripping onset and peak potentials, higher stability ($8\times$ improvement in stabilized oxidation current), and superior durability (by $1.6\times$) than the Pd black. In addition, a simple simulation of FAO was adopted to predict the anodic curve by including reaction intermediates of formate and hydroxyl. The 0 M-Au/Pd NPs were found to show higher formate and lower hydroxyl coverage than the Pd black.

© 2013 Elsevier B.V. All rights reserved.

1. Introduction

Direct formic acid fuel cells (DFAFCs) [1—3] appear as ideal portable power sources due to their unique features such as high open circuit voltage (1.45 V), allowable high concentration of fuel, and less fuel crossover through membranes compared to direct methanol fuel cells. To achieve efficient formic acid oxidation (FAO), bimetallic nanoparticles (NPs) [4—8] as the anode catalysts have been widely investigated. In these studies, Pd and Pd-based materials [9—11] are reported to achieve superior FAO activity than Pt-based materials.

The enhancement of catalytic activity is attributed to interactions between the metallic components, including geometric [12—14] and electronic contributions [15—17], which are commonly triggered by size, shape, morphology, interface and electronic structure. Core—shell bimetallic NPs [18—21] as one of the controllable structures that promote the above two contributions, not only demonstrate high catalytic activity, stability and durability, but also provide an ideal platform to explore the interaction between the core and shell. Among these core—shell structures, the Au/Pd NPs [22] exhibit superior electrochemical activity toward FAO. As is well known, the interaction between the core and shell strongly relies on interfacial stress, morphology and roughness of the core, etc.; however, the impact of roughness of the Au cores in the Au/Pd core—shell NPs has not been explored so far.

We have previously synthesized unique Au/Pd core—shell NPs by coating Pd on the surface of hollow Au nanospheres via an electrodeposition method [22—24]. The goal of this paper is to investigate the impact on catalytic ability toward FAO of the Au/Pd NPs synthesized using hollow Au cores with different surface roughness tuned by adjusting the concentration of Na_2SO_3 in the

* Corresponding author. 501 West First Street, Room 231, Engineering Laboratory Building, Arlington, TX 76019, USA. Tel.: +1 817 272 2704; fax: +1 817 272 2538.
E-mail address: fuqiang@uta.edu (F. Liu).

Au solution. A numerical simulation was also conducted to understand the difference in FAO reaction mechanisms between the Au/Pd core−shell NPs and commercial Pd black.

2. Experimental

2.1. Synthesis of Au/Pd NPs

The hollow Au/Pd core−shell NPs were fabricated from hollow Au spheres in an alumina membrane via an electrodeposition method according to our reported procedure [22−24]. Briefly, the Au^+ ions in the electrolyte were reduced into metallic hollow Au clusters at the boundary of hydrogen nanobubbles. Then Cu layers were coated onto the Au nanospheres in a Cu electrolyte. Subsequently, an aqueous solution of 2.53 mM $PdCl_2$ was used to replace the Cu layer through a galvanic reaction for 30 min. To tune the surface roughness of the hollow Au spheres according to our previous study [24,25], 1 ml Na_2SO_3 solution was added into 4 ml Au solution (7.775 g L^{-1}, Technic Inc.) at concentrations of 2 M, 0.2 M and 0 M (i.e. deionized water only) to form $[Au(SO_3)_2]^{3-}$ complexants. After leaving for 12 h, the final pH values of the mixed solution were 6.75, 6.3, and 6, for 2 M, 0.2 M, and 0 M, respectively. In this study, different Au/Pd NPs were labeled as 2 M, 0.2 M and 0 M accordingly.

2.2. Physical and electrochemical characterization

X-ray diffraction (XRD, Cu source) was used to identify the crystallinity of nanoparticles. Electronic configurations of the nanoparticles were probed by X-ray photoelectron spectroscopy (XPS, Perkin−Elmer Phi 560 XPS/Auger System with Al source). Field emission scanning electron microscopy (FE-SEM, Zeiss Supra 55 VP) was used to observe surface roughness of the nanoparticles. High-resolution transmission electron microscopy (HR-TEM, Hitachi H-9500) was applied to survey nanostructure of the catalysts. Composition of catalysts was examined by inductively coupled plasma mass spectrometry (ICP-MS, Perkin−Elmer ELAN DRC II ICP mass spectrometer system).
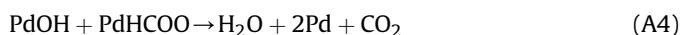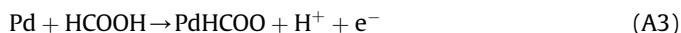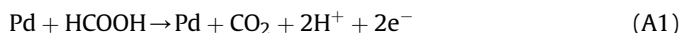
The electrochemical tests were performed on a Princeton Applied Research 2273 potentiostat in a three electrode configuration using a rotating disk electrode (Pine Instrument Company). Pt mesh and normal hydrogen electrode (NHE) were used as the counter electrode and reference electrode, respectively. Preparation of catalyst inks and rotating disk electrodes followed our reported procedure [26]. During CO-stripping measurement, CO was first adsorbed to the catalysts at 0.2 V for 900 s in a CO-saturated solution containing 0.1 M $HClO_4$. Subsequently, cyclic voltammetry (CV) was conducted from 0.075 V to 1.2 V at a rate of 10 mV s^{-1} after bubbling Ar for an hour. The FAO was studied in a mixed electrolyte (0.1 M $HClO_4$ and 0.1 M HCOOH) from −0.03 V to 1.4 V (vs. NHE) at a rotation speed of 1000 rpm. The chronoamperometric test was performed at 0.3 V for 3600 s in a mixed solution of 0.1 M $HClO_4$ and 0.1 M HCOOH. The catalytic durability was evaluated by an accelerated stress test (AST) protocol with square-wave potential cycles between 0.6 V (5 s) and 0.95 V (5 s) for 7000 and 14,000 cycles.

2.3. Simulation method

In order to study the FAO mechanism, we conducted a simple simulation by merely considering formate and hydroxyl groups as the intermediates [27,28], since several reports [29−34] already proved formate as the reaction intermediate during FAO reaction without generating CO as the poisoning species. Formate molecule was recently confirmed as one of the possible intermediates among others such as OH, $COOH_{ads}$ [35], and CHO_{ads} [36] via IR spectra and other techniques [29−34]. The electro-oxidation of formic acid on Pd-based catalysts is considered as a direct pathway via a dehydrogenation reaction (HCOOH → CO_2 + $2H^+$ + $2e^-$) [37]. During the reaction, the generated intermediates block the available sites on the catalysts and therefore prevent further reactions.

In this study, the possible reaction steps listed below are considered:

$$Pd + HCOOH \rightarrow Pd + CO_2 + 2H^+ + 2e^- \tag{A1}$$

$$H_2O + Pd \leftrightarrow PdOH + H^+ + e^- \tag{A2}$$

$$Pd + HCOOH \rightarrow PdHCOO + H^+ + e^- \tag{A3}$$

$$PdOH + PdHCOO \rightarrow H_2O + 2Pd + CO_2 \tag{A4}$$

These four equations consist of one direct dehydrogenation pathway (A1) and other intermediate-containing pathways. Here, the coverage of the formate and hydroxyl group was denoted as θ_1 and θ_2, respectively. The corresponding kinetic equations for the above reactions can be expressed as follows [27,38]:

$$V_1 = k_1 C_f (1 - \theta_1 - \theta_2) \exp\left(\frac{E}{b_1}\right) \tag{B1}$$

$$V_2 = k_2 C_w (1 - \theta_1 - \theta_2) \exp\left(\frac{E}{b_2}\right) - k_{-2} C_{H^+} \theta_2 \exp\left(\frac{-E}{b_2}\right) \tag{B2}$$

$$V_3 = k_3 C_f (1 - \theta_1 - \theta_2) \exp\left(\frac{E}{b_3}\right) - k_{-3} C_{H^+} \theta_1 \exp\left(\frac{-E}{b_3}\right) \tag{B3}$$

$$V_4 = k_4 \theta_1 \theta_2 C_f C_{H^+} \tag{B4}$$

where E is the potential (V vs. NHE), C is the concentration (M) with subscripts representing different species (e.g., f: formic acid; w: water), b is the Tafel slope, and k is the reaction constant. Table 1 lists parameters for the Au/Pd NPs and Pd black. The overall production rates of formate and hydroxyl can be calculated by the following equations:

$$q \cdot \frac{d\theta_1}{dt} = V_3 - V_4 \tag{B5}$$

$$q \cdot \frac{d\theta_2}{dt} = V_2 - V_4 \tag{B6}$$

Table 1
Parameters of simulation model ([27,43]).

Parameters	Values (Au/Pd NPs)	Values (Pd black)	Unit
Scan range	0−1.4	0−1.4	V
Scan rate	10	10	mV s^{-1}
k_1	1.0×10^{-3}	3.2×10^{-4}	A cm^{-2} M^{-1}
k_2	3.3×10^{-5}	3.3×10^{-5}	A cm^{-2} M^{-1}
k_{-2}	60	60	A cm^{-2} M^{-1}
k_3	1.0×10^{-5}	1.0×10^{-5}	A cm^{-2} M^{-1}
k_{-3}	9×10^{-7}	9×10^{-7}	A cm^{-2} M^{-1}
k_4	4.0×10^{-3}	4.0×10^{-3}	A cm^{-2} M^{-1}
C_w	55.6	55.6	M
q	0.02016	0.02016	C cm^{-2}
C_f	0.1	0.1	M
C_H	0.1	0.1	M
b_1	0.19	0.16	V
b_2	0.18	0.15	V
b_3	0.18	0.15	V

in which q is assumed to be the charge of these intermediates absorbed on the Pd surface. Finally, the total current density ($J = \text{mA cm}^{-2}$) can be calculated as:

$$J = 2 \cdot V_1 + V_2 + V_3 \tag{B7}$$

3. Results and discussion

XRD patterns of commercial Pd black (Alfa Aesar) in Fig. 1 show Pd (111), (200), (220) and (311) planes at 40.20°, 46.73°, 68.21° and 82.17°, respectively. For the three Au/Pd NPs obtained using different Na_2SO_3 concentration indicated in the figure, the peaks at 38.44°, 44.45°, 64.88°, 77.71°, 81.88° correspond respectively to Au (111), (200), (220), (311), and (222) planes (JCPDS No. 04-0784; 38.18°, 44.39°, 64.57°, 77.54°, 81.72°). Because of highly dispersed Pd nanocrystallites embedded at the Au surface (will be shown in TEM images in Fig. 4), the Au/Pd NPs display very weak Pd signal in Fig. 1. In addition, there is no identifiable Cu signal in the spectra, suggesting that Cu has been completely replaced by the Pd shell.

Fig. 2 shows the Pd 3d core-level XPS spectra of the Au/Pd NPs and Pd black. From XPS result, not only the electronic configuration of Pd was probed, but also the presence of nanocrystalline Pd can be confirmed. The Au/Pd NPs of 0 M, 0.2 M, and 2 M show lower Pd $3d_{5/2}$ binding energy at 334.9 eV, 334.9 eV, and 335.4 eV, respectively, than the Pd black (335.5 eV). The impact of the core-level binding energy on electrochemical FAO will be examined in Fig. 5.

Fig. 3 shows the FE-SEM images of the three types of hollow Au nanospheres. The average particle size in diameter is about 120 nm for 0 M, 100 nm for 0.2 M and 90 nm for 2 M. It is found that the surface roughness of the three Au NPs ranks in the order of 2 M > 0.2 M > 0 M, indicating that $[SO_3]^{2-}$ plays an important role to stabilize Au ions in the solution and alter the hollow Au morphologies. Our previous study has discovered that the size and roughness of the Au NPs critically depend on the Au ions in various $[Au(SO_3)_2]^{3-}$ complexants and smoother surface of Au NPs could be achieved by adding lower concentration of Na_2SO_3 solution [25].

The microstructures of the hollow Au/Pd NPs synthesized in different Na_2SO_3 concentrations were investigated by HR-TEM in Fig. 4. The image of Fig. 4(a) clearly displays a continuous 10 nm-thick Pd shell and the average size of Au/Pd NPs is around 130 nm in diameter. In addition, the TEM images of the 0.2 M and 2 M Au/Pd
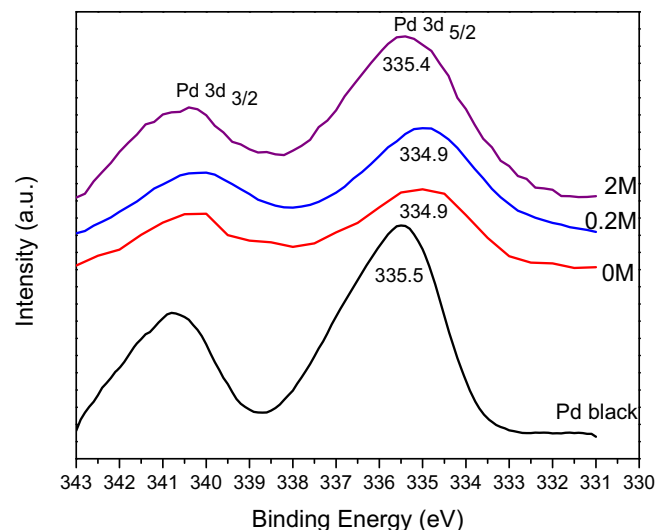

Fig. 2. Pd 3d XPS spectra of four Au/Pd NPs and Pd black.

NPs in Fig. 4b and c, respectively, indicate that their sizes are around 115 and 120 nm in diameter. The island-like Pd shells of the 0.2 M and 2 M Au/Pd NPs show observably higher roughness than 0 M-Au/Pd NPs. With increasing Na_2SO_3 concentration in the Au solution, the roughness of the Au nanospheres increases, and thus impedes continuous Pd growth on the surface of Au.

Electrochemical characteristics of the Au/Pd NPs and Pd black were evaluated in Fig. 5. The current densities have been normalized to the electrochemical surface area (ECSA). ECSA ($m^2 \, g_{Pd}^{-1}$) was calculated from the hydrogen adsorption after correcting the double-layer charges and then divided by the Pd mass (identified by ICP-MS). The calculated ECSA is individually listed: 2 M: $6.61 \, m^2 \, g^{-1}$, 0.2 M: $6.54 \, m^2 \, g^{-1}$, 0 M: $4.5 \, m^2 \, g^{-1}$ and Pd black: $6.3 \, m^2 \, g^{-1}$. The CO-stripping results in Fig. 5(a) show that the 0 M-Au/Pd NPs display the lowest CO oxidation peak potential at 0.82 V compared to the Pd black (0.95 V), 0.2 M (0.91 V) and 2 M (0.90 V) Au/Pd NPs. Besides, the Au/Pd NPs display lower onset potential for CO oxidation with the 0 M sample being almost 0.2 V lower than that of the Pd black, indicating the strongest CO oxidation ability and electronic coupling between the Au core and Pd shell. On the other hand, the availability of higher coordination Pd sites (the most stable configuration) might be slightly reduced for smaller Pd particles (Au/Pd NPs ~6—10 nm; Pd black ~15 nm). Since the CO-stripping is a structure sensitive technique, the broadening of CO-stripping peak of the Au/Pd NPs may result from different bonds of CO to the catalysts such as linear, bridge and others [39].

It is well known that CO or CO-like intermediates may retard the activities of catalysts and the FAO kinetics strongly depend on oxidation of these intermediates on the core—shell NPs at lower potential. Fig. 5(b) shows that the 0 M-Au/Pd NPs demonstrate the highest area-specific current density ($6.5 \, \text{mA cm}^{-2}$) in the forward scan direction while the Pd black only shows a peak current of $1.93 \, \text{mA cm}^{-2}$. The specific activity ($1.01 \, \text{mA cm}^{-2}$) of the 0 M-Au/Pd NPs measured at 0.3 V (the normal working potential in a DFAFC) almost doubles that of the Pd black ($0.51 \, \text{mA cm}^{-2}$). In addition, the 0 M-Au/Pd NPs showed the highest peak potential (0.736 V) in both the anodic and cathodic scans. Since the catalytic oxidation is highly structure-sensitive [40], the defects and steps in the Pd shell, caused by rougher Au core, are easy to adsorb anions and prone to be poisoned, thus inhibiting the FAO reaction. Moreover, the electronic interaction [41,42] between Au support and Pd catalyst may influence the catalytic activity. The XPS result of 2 M
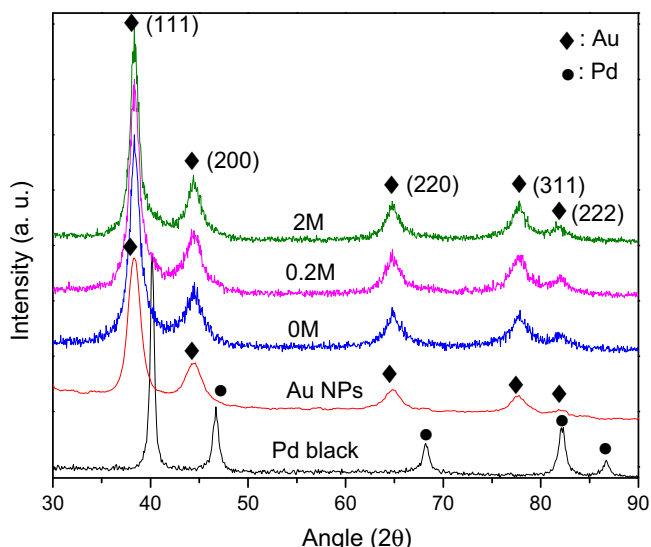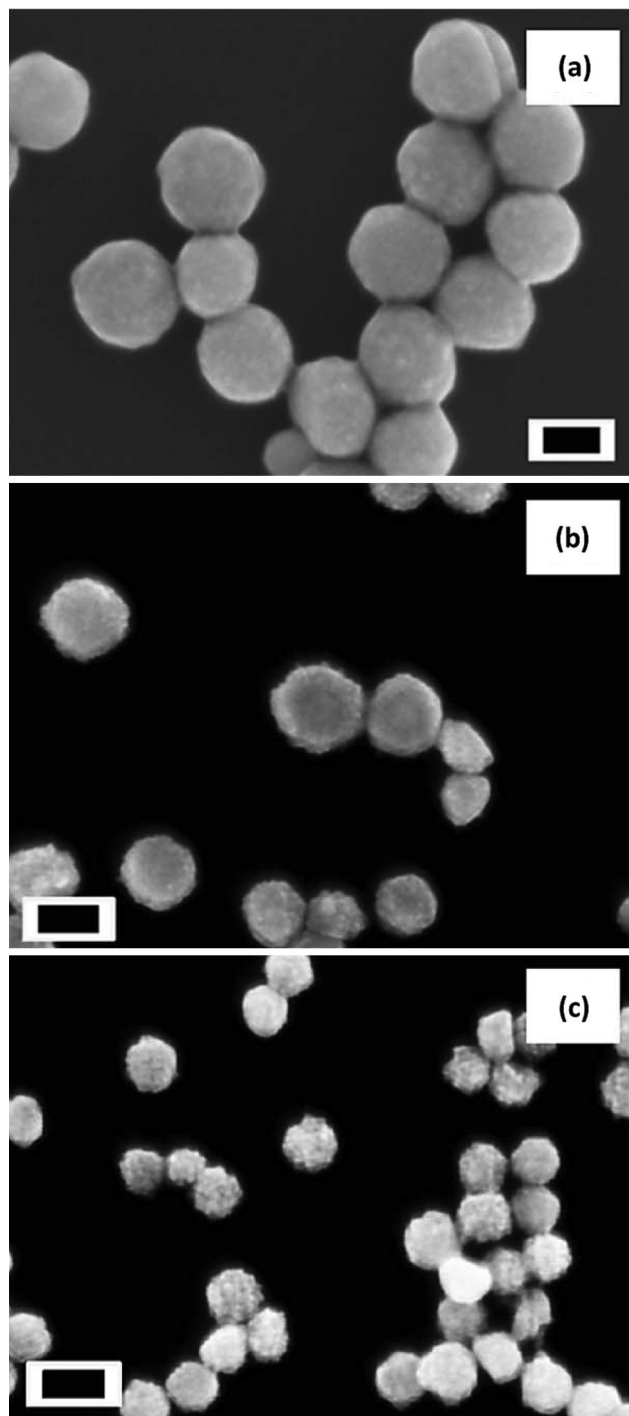

Fig. 1. XRD pattern of Au/Pd NPs and Pd black.

Fig. 3. FE-SEM images of different Au NPs, (a) 0 M; (b) 0.2 M and (c) 2 M. The scale is 100 nm.

Fig. 4. HR-TEM images of different Au/Pd NPs, (a) 0 M; (b) 0.2 M and (c) 2 M.

Au/Pd NPs in Fig. 2 demonstrated a positive shift of the binding energy (broad peak, 335.7–335.1 eV), suggesting a lower FAO activity according to the Refs. [22,43]. This may explain why the 2 M Au/Pd NPs show lower catalytic activity than other Au/Pd NPs and Pd black.

The FAO stability of the Au/Pd NPs and Pd black was studied by the chronoamperometry tests in Fig. 5(c). The 0 M-Au/Pd NP shows the highest area-specific current density initially and is able to maintain its superior perfor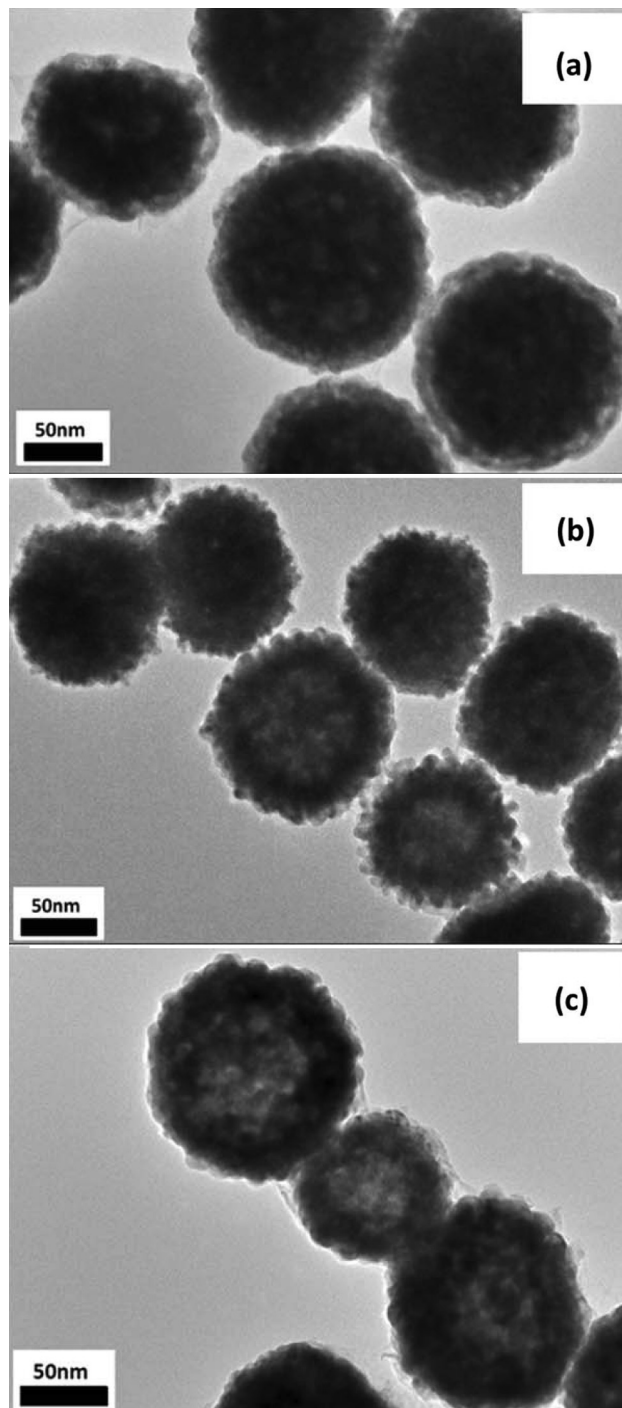mance even after 1 h at 0.064 mA cm^{-2} which is obviously higher than those of the Pd black (0.008 mA cm^{-2}) and other Au/Pd NPs. Durability of the Au/Pd NPs was evaluated under the AST protocol with potentials applied between 0.6 V (5 s) and 0.95 V (5 s) up to 14,000 cycles. Fig. 5(d) shows that the 0 M-Au/Pd NPs preserves almost 84% of its initial ECSA in the first 7000 cycles and 60% after 14,000 cycles; however, the ECSA loss for the Pd black is 35% in the first 7000 cycles and 62.4% after 14,000 cycles. The 0.2 M and 2 M-Au/Pd NPs also demonstrate better electrochemical durability in the long-term AST than the Pd black. Generally, in terms of most favorable particle size of Pd nanoparticles for FAO, an intermediate range between 5-7 nm
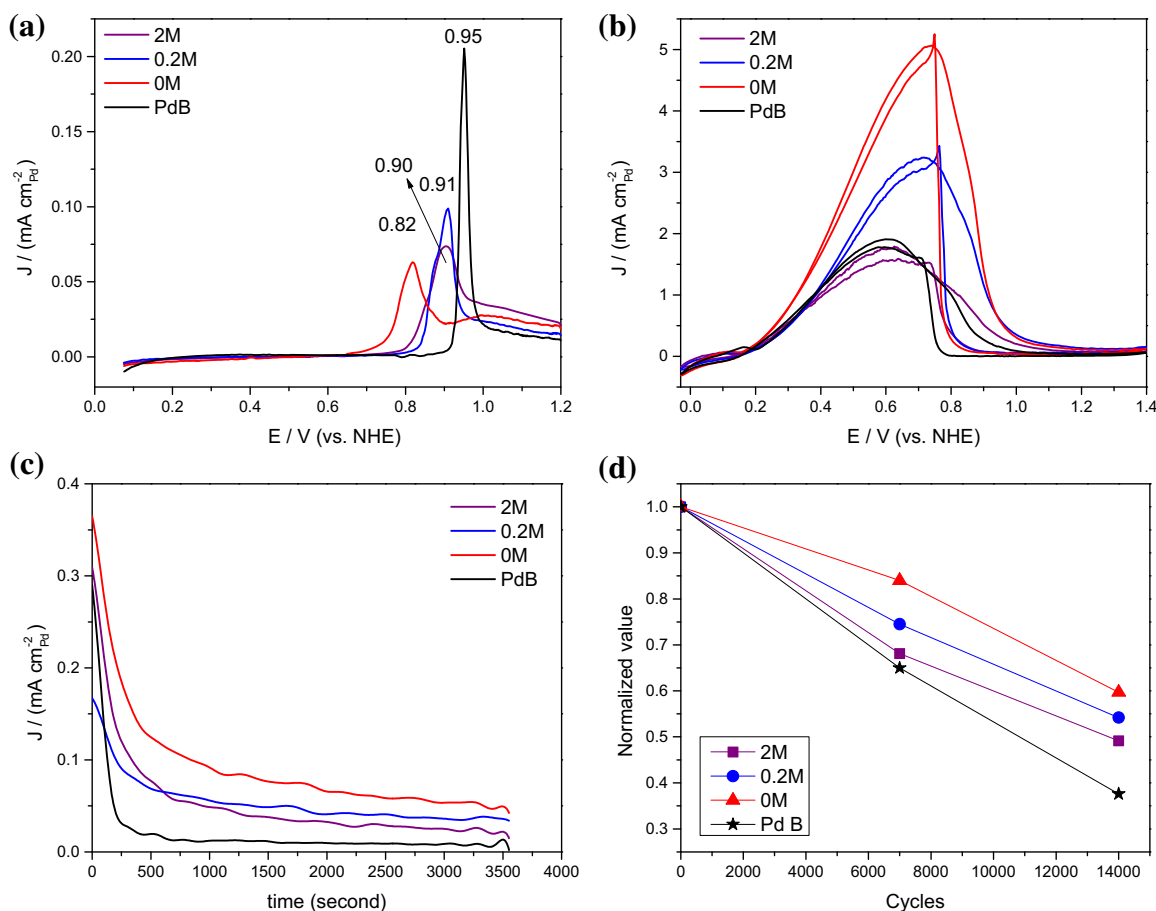
Fig. 5. Electrochemical characterization of the Au/Pd NPs and Pd black, (a) CO-stripping CV of Pd catalysts in HClO$_4$ solution; (b) CV of formic acid oxidation of Au/Pd and Pd black in 0.1 M of HClO$_4$ and HCOOH solution at 1000 rpm; (c) chronoamperometry curves in 0.1 M of HClO$_4$ and HCOOH solution at 0.3 V up to 3600 s; and (d) normalized ECSA of Pd catalysts after 7 k (19.4 h) and 14 k (38.89 h) cycles of AST. The scan rate for the whole test was applied at 10 mV/s.

is most active as reported by Zhou et al. [39]. In this study, we believe that the Pd grains in the shell of different samples remain within that favorable range (as confirmed by HR-TEM images). Under constant Pd particle size, changes in Pd surface structure and electronic effects, both induced by roughness of the Au core, play a key role in both catalytic activity and durability. It is well known that during long-term tests in an acid environment, PdO and PdOH species will be generated leading to a decrease of efficiency and possible corrosion of the Pd catalysts. The 0 M-Au/Pd NPs express higher stability and durability which may be due to fewer defects on Pd layers and lower Pd 3d core-level binding energy [44]; therefore, both geometric and electronic effects originated from the smooth Au core in the 0 M-Au/Pd NPs may contribute to its superior durability.

To understand the FAO mechanism and shed light on the fundamental difference between Au/Pd NPs and Pd black, numerical simulation is adopted in this study. Fig. 6(a) shows the anodic scan of the simulated (dot-line) and experimental curves (solid-line) of the 0 M-Au/Pd NPs and Pd black. It is apparent that the simulation result agrees well with the experimental result, except that at higher potential the curve of the Au/Pd NPs after peak potential drops suddenly probably due to accumulation of intermediates on the reactive surface (blocking-site effect). The corresponding parameters used in the simulation shown in Table 1 indicate that the reaction constant k_1 of the Au/Pd NPs is higher than that of Pd black while other reaction constants are unchanged. This suggests that the FAO reaction majorly happens in

dehydrogenation pathway, in a good agreement with reports in literature [29,32] that HCOOH$_{ads}$ forms on Pd surface and carries the most oxidation current.

The kinetics of electrochemical reactions strongly depends on the charge transfer coefficient which is closely related to the electrode material. The charge transfer coefficient (α) [45] is calculated from: $\alpha = 2.303 \times R \times T/(n \times b \times F)$, where R is the gas constant, T is the absolute temperature, n is the number of electrons, b is the Tafel slope and F is the Faraday constant. The transfer coefficient from the Tafel slope (b_1) of the Au/Pd NPs (0.155) is smaller than that of the Pd black (0.184) with assumption of $n = 2$. Also, the transfer coefficients calculated from b_2 and b_3 ($n = 1$) are smaller for the Au/Pd NPs ($\alpha = 0.328$) than those of the Pd black ($\alpha = 0.394$). In addition, the surface coverage of the formate and hydroxyl groups on the Au/Pd NPs and Pd black in Fig. 6(b) and (c) show much lower formate coverage than those of hydroxyl group, which agrees with reported results in many studies using infrared technique. For example, Samjeske et al. [33] reported that formate was generated at low potentials and reached to the highest coverage at around 1.0 V similar to Miyake's finding [32] (highest peak at 0.8 V). However, signal of the formate in many reports shows very low intensity due to its low coverage on the catalyst surface. Chen et al. [46] reported that 15% of FAO current is attributed from oxidation of formate, and the rest may come from reactions in other pathways. The result of the Au/Pd NPs in Fig. 6(b) shows that formate starts forming on the surface of the catalysts at 0.01 V and reaches to a surface coverage of 6.8% at 1.1 V; however, the hydroxyl group starts to generate at
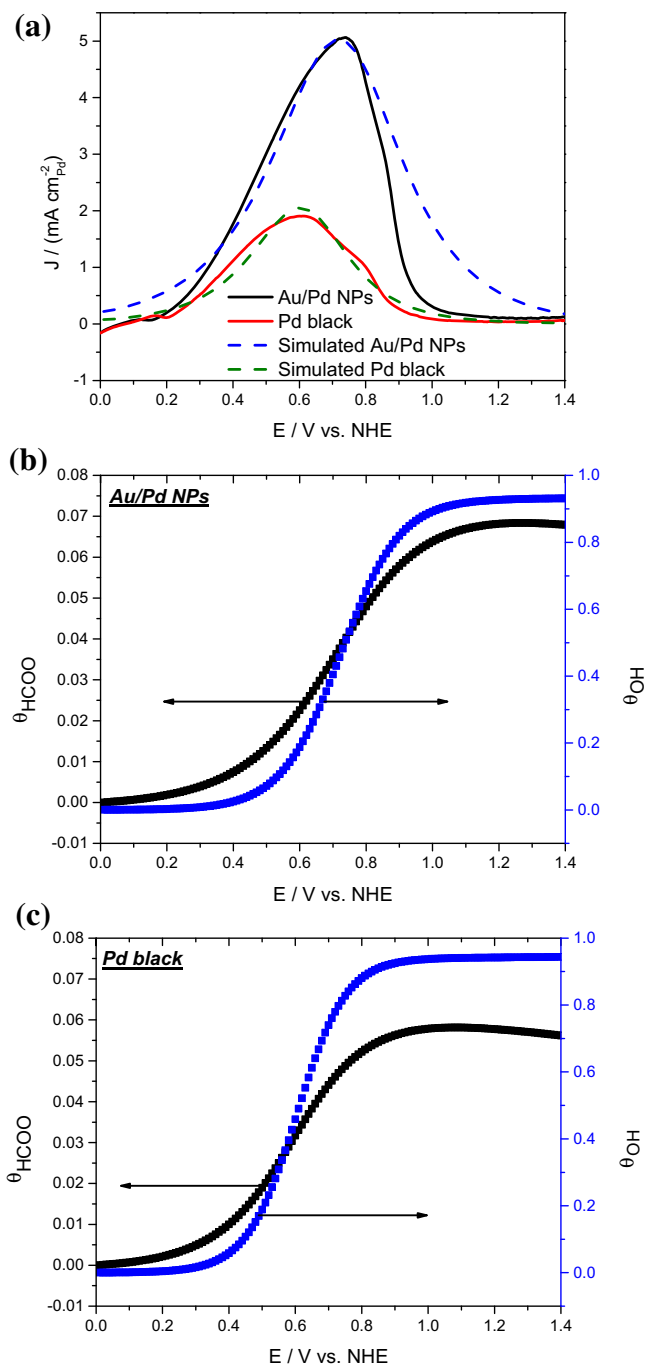
Fig. 6. (a) Comparison of experimental (solid-line) and simulated (dot-line) results of the Au/Pd NPs and Pd black. The simulated surface coverage of formate and hydroxyl group for (b) Au/Pd NPs and (c) Pd black in different potentials, respectively.

0.3 V and reaches to 93% coverage at 1.2 V. For the Pd black in Fig. 6(c), formate forms at 0.01 V and achieves 5.8% coverage at 1.0 V, and slightly decreases with increasing potential; the hydroxyl group begins to accumulate on the surface at 0.3 V and reach to 94% coverage at 1.0 V. Comparison between the Au/Pd NPs and Pd black suggests higher formate and lower hydroxyl coverage on the Au/Pd NPs especially at higher potentials. Most important, hydroxyl adsorption on Au/Pd NPs has been remarkably delayed. For example, the hydroxyl coverage of 0.1, i.e., $\theta_{OH} = 0.1$, occurs at ca. 0.59 V for the Au/Pd NPs but at 0.48 V for the Pd black. Since hydroxyl group on the Pd surface (PdOH), as a product of surface

oxidation, has been widely considered as a poisoning species which would inhibit the catalytic activity. As a result, the anti-oxidation property of the Au/Pd NPs promotes both electrochemical activity toward FAO and durability of Pd during the AST.

4. Conclusions

We have synthesized the Au/Pd core–shell NPs using different hollow Au nanospheres with different surface roughness. The higher concentration of Na_2SO_3 in the Au solution generated rougher Au surface; however, the defects of the Pd layer on the Au/Pd core–shell structure are expected to increase accordingly. These defects may retard the electrochemical reaction of FAO on the catalysts. From the electrochemical results, our Au/Pd core–shell NPs show superior catalytic activities for FAO, stability, CO oxidation ability and long-term durability than the Pd black. Particularly, the 0 M-Au/Pd NPs synthesized in this study present the best catalytic properties probably due to fewer defects in the Pd layer. In order to further understand the experimental results, we developed a simple model, which aims to provide insights to the FAO reaction mechanism. The simulation result of the 0 M-Au/Pd NPs shows a higher formate coverage and smaller hydroxyl group coverage than those of the Pd black. In addition, the kinetic reaction current of FAO is dependent on the catalytic ability to remove these formate and hydroxyl groups.

References

[1] Y. Zhu, S.Y. Ha, R.I. Masel, J. Power Sources 130 (2004) 8–14.
[2] K.-J. Jeong, C.M. Miesse, J.-H. Choi, J. Lee, J. Han, S.P. Yoon, S.W. Nam, T.-H. Lim, T.G. Lee, J. Power Sources 168 (2007) 119–125.
[3] S.M. Baik, J. Kim, J. Han, Y. Kwon, Int. J. Hydrogen Energy 36 (2011) 12583–12590.
[4] S. Zhang, M. Qing, H. Zhang, Y. Tian, Electrochem. Commun. 11 (2009) 2249–2252.
[5] Q. Yi, A. Chen, W. Huang, J. Zhang, X. Liu, G. Xu, Z. Zhou, Electrochem. Commun. 9 (2007) 1513–1518.
[6] C. Rice, S. Ha, R.I. Masel, A. Wieckowski, J. Power Sources 115 (2003) 229–235.
[7] X. Ji, K.T. Lee, R. Holden, L. Zhang, J. Zhang, G.A. Botton, M. Couillard, L.F. Nazar, Nat. Chem. 2 (2010) 286–293.
[8] G. Chen, Y. Li, D. Wang, L. Zheng, G. You, C.-J. Zhong, L. Yang, F. Cai, J. Cai, B.H. Chen, J. Power Sources 196 (2011) 8323–8330.
[9] X. Wang, Y. Tang, Y. Gao, T. Lu, J. Power Sources 175 (2008) 784–788.
[10] X. Gu, Z.-H. Lu, H.-L. Jiang, T. Akita, Q. Xu, J. Am. Chem. Soc. 133 (2011) 11822–11825.
[11] J.-H. Choi, K.-J. Jeong, Y. Dong, J. Han, T.-H. Lim, J.-S. Lee, Y.-E. Sung, J. Power Sources 163 (2006) 71–75.
[12] O.M. Wilson, M.R. Knecht, J.C. Garcia-Martinez, R.M. Crooks, J. Am. Chem. Soc. 128 (2006) 4510–4511.
[13] K.J.J. Mayrhofer, B.B. Blizanac, M. Arenz, V.R. Stamenkovic, P.N. Ross, N.M. Markovic, J. Phys. Chem. B 109 (2005) 14433–14440.
[14] A.L. Dantas Ramos, P.d.S. Alves, D.A.G. Aranda, M. Schmal, Appl. Catal. A: Gen. 277 (2004) 71–81.
[15] A.M. Venezia, A. Rossi, L.F. Liotta, A. Martorana, G. Deganello, Appl. Catal. A: Gen. 147 (1996) 81–94.
[16] A. Sarkany, Z. Zsoldos, G. Stefler, J.W. Hightower, L. Guczi, J. Catal. 157 (1995) 179–189.
[17] M. Chen, D. Kumar, C.-W. Yi, D.W. Goodman, Science 310 (2005) 291–293.
[18] P. Strasser, S. Koh, T. Anniyev, J. Greeley, K. More, C. Yu, Z. Liu, S. Kaya, D. Nordlund, H. Ogasawara, M.F. Toney, A. Nilsson, Nat. Chem. 2 (2010) 454–460.
[19] V. Mazumder, M. Chi, K.L. More, S. Sun, J. Am. Chem. Soc. 132 (2010) 7848–7849.

[20] J. Luo, M.M. Maye, Y. Lou, L. Han, M. Hepel, C.J. Zhong, Catal. Today 77 (2002) 127–138.
[21] S. Alayoglu, A.U. Nilekar, M. Mavrikakis, B. Eichhorn, Nat. Mater. 7 (2008) 333–338.
[22] C. Hsu, C. Huang, Y. Hao, F. Liu, Electrochem. Commun. 23 (2012) 133–136.
[23] C. Hsu, C. Huang, Y. Hao, F. Liu, Phys. Chem. Chem. Phys. 14 (2012) 14696–14701.
[24] C. Hsu, C. Huang, Y. Hao, F. Liu, Nanoscale Res. Lett. 8 (2013) 113.
[25] C. Huang, Y. Hao, J. Nanosci. Nanotechnol. 11 (2011) 3701–3705.
[26] S. Patel, J. Jiang, F. Liu, Int. J. Hydrogen Energy 36 (2011) 11108–11115.
[27] X. Wang, J.-M. Hu, I.M. Hsing, J. Electroanal. Chem. 562 (2004) 73–80.
[28] J. Xu, D. Yuan, F. Yang, D. Mei, Z. Zhang, Y.-X. Chen, Phys. Chem. Chem. Phys. 15 (2013) 4367–4376.
[29] Y.X. Chen, M. Heinen, Z. Jusys, R.J. Behm, Angew. Chem. Int. Ed. 45 (2006) 981–985.
[30] G.-Q. Lu, A. Crown, A. Wieckowski, J. Phys. Chem. B 103 (1999) 9700–9711.
[31] A. Miki, S. Ye, M. Osawa, Chem. Commun. (Cambridge, UK) (2002) 1500–1501.
[32] H. Miyake, T. Okada, G. Samjeske, M. Osawa, Phys. Chem. Chem. Phys. 10 (2008) 3662–3669.
[33] G. Samjeské, A. Miki, S. Ye, M. Osawa, J. Phys. Chem. B 110 (2006) 16559–16566.
[34] G. Samjeské, M. Osawa, Angew. Chem. Int. Ed. 44 (2005) 5694–5698.
[35] S.G. Sun, J. Clavilier, A. Bewick, J. Electroanal. Chem. Interfaces 240 (1988) 147–159.
[36] S. Wilhelm, W. Vielstich, H.W. Buschmann, T. Iwasita, J. Electroanal. Chem. Interfaces 229 (1987) 377–384.
[37] N.M. Marković, H.A. Gasteiger, P.N. Ross Jr., X. Jiang, I. Villegas, M.J. Weaver, Electrochim. Acta 40 (1995) 91–98.
[38] J.D. Lović, A.V. Tripković, S.L. Gojković, K.D. Popović, D.V. Tripković, P. Olszewski, A. Kowal, J. Electroanal. Chem. 581 (2005) 294–302.
[39] W. Zhou, J.Y. Lee, J. Phys. Chem. C 112 (2008) 3789–3793.
[40] M. Koper, Fuel Cell Catalysis: a Surface Science Approach, John Wiley & Sons Inc., New Jersey, 2009.
[41] T. Cheng, E. Gyenge, J. Appl. Electrochem. 39 (2009) 1925–1938.
[42] M.K. Debe, Nature 486 (2012) 43–51.
[43] J.C. Bertolini, P. Delichere, B.C. Khanra, J. Massardier, C. Noupa, B. Tardy, Catal. Lett. 6 (1990) 215–223.
[44] J. Wang, G. Yin, Y. Shao, Z. Wang, Y. Gao, J. Phys. Chem. C 112 (2008) 5784–5789.
[45] Y. Liu, L. Wang, G. Wang, C. Deng, B. Wu, Y. Gao, J. Phys. Chem. C 114 (2010) 21417–21422.
[46] Y.X. Chen, M. Heinen, Z. Jusys, R.J. Behm, Langmuir 22 (2006) 10399–10408.